

VIRIAL INFECTIONS: REPLICATION  
AND PATHOGENESIS MECHANISMS TO THERAPY

UDC 578.286; 57.084.1

## Generation of SARS-CoV-2 Mouse Model by Transient Expression of the Human *ACE2* Gene Mediated by Intranasal Administration of AAV-hACE2

D. V. Glazkova<sup>a</sup>, E. V. Bogoslovskaya<sup>a</sup>, F. A. Urusov<sup>a, b, \*</sup>, N. P. Kartashova<sup>c</sup>,  
E. A. Glubokova<sup>c</sup>, A. V. Gracheva<sup>c</sup>, E. B. Faizuloev<sup>c</sup>, G. V. Trunova<sup>d</sup>, V. A. Khokhlova<sup>d</sup>,  
O. A. Bezborodova<sup>d</sup>, A. A. Pankratov<sup>d</sup>, I. A. Leneva<sup>c</sup>, and G. A. Shipulin<sup>a</sup>

<sup>a</sup> Center for Strategic Planning and Management of Medical and Biological Health Risks,  
Federal Medical-Biological Agency of the Russian Federation, Moscow, 119992 Russia

<sup>b</sup> Izmerov Research Institute of Occupational Health, Moscow, 105275 Russia

<sup>c</sup> Mechnikov Research Institute of Vaccines and Sera, Moscow, 105064 Russia

<sup>d</sup> National Medical Research Radiological Centre, Ministry of Health of the Russian Federation, Moscow, 125284 Russia

\*e-mail: flanger.fx@mail.ru

Received January 25, 2022; revised April 8, 2022; accepted April 12, 2022

**Abstract**—One of the most important steps in the development of drugs and vaccines against a new coronavirus infection is their testing on a relevant animal model. The laboratory mouse, with well-studied immunology, is the preferred mammalian model in experimental medicine. However, mice are not susceptible to infection with SARS-CoV-2 due to the lack of human angiotensin-converting enzyme (hACE2), which is the cell receptor of SARS-CoV-2 and necessary for the entry of the virus into the cell. In present work, it was shown that intranasal administration of the adeno-associated vectors AAV9 and AAV-DJ encoding the hACE2 provided a high level of expression of *ACE2* gene in the lungs of mice. In contrast, the introduction of the AAV6 vector led to a low level *ACE2* expression. Infection with SARS-CoV-2 of mice expressing hACE2 in the lungs led to virus replication and development of bronchopneumonia on the 7th day after infection. Thus, a simple method for delivering the human *ACE2* gene to mouse lungs by intranasal administration of the AAV vector has been proposed. This approach enabled rapid generation of mouse model for studying coronavirus infection.

**Keywords:** hACE2, SARS-CoV-2, AAV9, AAV6, AAV-DJ, BALB/c mice

**DOI:** 10.1134/S0026893322050065

For the development and testing of therapeutic and prophylactic drugs against any infection, including the new coronavirus infection, COVID-19, relevant animal models must be used. The most common and available animals—laboratory mice—cannot be used to model disease caused by the SARS-CoV-2 virus. This is because SARS-CoV-2 virions need a cellular receptor, human angiotensin-converting enzyme-2 (hACE2), to enter the host cell and begin its infectious cycle. The mouse orthologue of hACE2 (*Ace2*) is not recognized by this coronavirus, that is, it does not serve as its receptor, and therefore SARS-CoV-2 cannot infect mouse cells. The emergence in 2021 of transgenic mice in which the hACE2 gene, *ACE2*, is present in the genome and expressed in lung cells, partly solves this problem [1]. However, these animals are not always available and, moreover, are limited to a line with a specific genetic background, which does not allow study of the influence of genetic characteristics

on the disease. A simpler and more affordable solution could be to introduce a vector carrying the *ACE2* gene into mice lungs. Hassan A. et al. [2] showed that intranasal administration of an adenoviral vector (AdV) encoding hACE2 makes it possible to achieve the expression of this protein in the lungs of mice and to obtain animals susceptible to SARS-CoV-2 infection. However, the introduction of AdV is accompanied by an inflammatory process in the bronchi, which can distort the picture of the course of COVID-19 infection during subsequent infection. The use of adeno-associated viral vectors (AAV vectors) that do not cause inflammation was also proposed for *ACE2* gene delivery, although in this case only intratracheal injection of the AAV vector into the respiratory tract of mice proved to be effective [3, 4]. It should be noted that intratracheal administration is an invasive method which greatly complicates the production of transduced animals. Based on these facts, we set our-

selves the task of optimizing *ACE2* gene delivery using AAV vectors into the respiratory tract of BALB/c mice and characterizing an experimental model of COVID-19 infection in these laboratory animals.

## EXPERIMENTAL

**Viruses, cells.** HEK-293FT cells (Invitrogen, United States) were cultured in DMEM medium (Gibco, United States) containing 10% fetal bovine serum (FBS; Gibco) and 0.01 M HEPES (Gibco). Cell line Vero CCL81 (ATCC, USA) from the collection of the I.I. Mechnikov Research Institute of Vaccines and Serums (Russia) was cultured in DMEM medium with 5% FBS, 100 IU/mL penicillin, and 100 µg/mL streptomycin. The Dubrovka SARS-CoV-2 laboratory strain (GenBank Acc. No. MW161041.1) was isolated on a Vero CCL81 cell culture from a nasopharyngeal swab from a COVID-19 patient. The strain underwent 20 consecutive passages on Vero CCL81 cells and produced a pronounced cytopathic effect.

**Construction of plasmid pAAV-hACE2.** The plasmid pcDNA3-sACE2(WT)-Fc(IgG1) containing the N-terminal part of the gene *ACE2*, encoding the hACE2 protein, was obtained from Addgene (Addgene plasmid #154104) [5]. Assembly of the C-terminal part was carried out by overlap extension PCR [6]. The overlapping N- and C-terminal regions were amplified and assembled using PCR. The fragment containing the complete gene was integrated into the pAAV-GFP plasmid vector (CellBioLabs, Inc., USA) to obtain the pAAV-hACE2 plasmid, which was validated by sequencing.

**Preparation of AAV-hACE2 vector particles.** The helper plasmid pHelper (CellBioLabs, Inc.), the vector plasmid pAAV-hACE2, and one of the pAAV6-RC6, pAAV9-RC, or pAAVDJ-RC plasmids encoding AAV serotype 6, 9, or DJ capsid proteins were used to generate AAV vectors (CellBioLabs, Inc.). Vector particles were prepared and purified using the polyethyleneimine transfection and polyethylene glycol (PEG 8000) purification protocol described by T. Kimura et al. [7].

**AAV titer determination by PCR.** To determine the AAV titer (the number of vector genomes per 1 mL, vg/mL), DNA was isolated from the sample using the AmpliTest RIBO-prep reagent kit (Federal State Budgetary Institution “Center for Strategic Planning and Management of Medical and Biological Health Risks” Federal Medical and Biological Health Risk Management Agency of Russia, Russia) in accordance with the manufacturer’s recommendations. Real-time PCR was performed on a RotorGene Q instrument using primers for the AAV ITR region and an appropriate amplification program [8].

**Experimental animals.** The study used female mice of the BALB/c line weighing 18–20 g, which were obtained from BioNursery STESAR (Russia).

**Introduction of AAV-hACE2 vector.** A suspension of vector particles was administered intranasally to mice in a total volume of 60 µL (30 µL in each nostril) under light ether anesthesia, keeping the animals at an angle of 45° with the mouth fixed in the closed position [9].

**Infection of animals.** Mice were infected with the SARS-CoV-2 virus, taken in a titer of  $3.2 \times 10^6$  TCID<sub>50</sub>/mL, intranasally: total volume—60 µL (30 µL in each nostril)—under light ether anesthesia. Animals included in the comparison groups were intranasally administered phosphate-buffered saline in the same way and in the same volume.

**Determination of the infectious titer of the virus in the lungs.** Hereinafter, the material for research was obtained from animals humanely killed under anesthesia. Lungs were removed under sterile conditions, which were homogenized and resuspended in phosphate-buffered saline. The suspension was clarified by centrifugation. Vero CCL81 cells were seeded into 96-well plates (Costar, United States) at a density of  $2 \times 10^4$  cells per well and cultured for 3 days. 10-fold dilutions of virus samples from the lungs were prepared, which were added to the wells of the plate (200 µL/well) and incubated at 37°C for 5 days until a cytopathic effect appeared in the virus control cells. The calculation of the virus titer was carried out according to the method described by MA Ramakrishnan [10] and expressed in lg (TCID<sub>50</sub>/mL). The sensitivity limit of the method was 1.5 lg.

**Extraction of RNA from mouse lung samples.** Lungs were removed and homogenized under sterile conditions in 1 mL of ExtractRNA solution (Evrogen, Russia). The lysate was clarified by centrifugation and the RNA was extracted with chloroform. Next, RNA was isolated using the AmpliTest RIBO-prep reagent kit (Federal State Budgetary Institution “Center for Strategic Planning and Management of Medical and Biological Health Risks” of the Federal Medical and Biological Health Organization of Russia) according to the manufacturer’s recommendations.

**ACE2 gene expression analysis in the lungs of mice.** RNA samples were treated with DNase for 20 min, after which they were heated at 70°C for 10 min. The amount of hACE2 mRNA in the samples was determined by real-time PCR using the primers: 5'-CTG-GGAATCCAACCAACTCTG-3', 5'-CCACTACAA-TCACGTCCATC-3' and the probe 5'-Fam-CCAGC-CCCCGTTAGTATTTGGCTC-BHQ1-3'. As an internal control, real-time PCR with primers for the mouse beta-glucuronidase gene (*Gusb*) was used.

**Determination of SARS-CoV-2 RNA in the lungs.** RNA samples were tested for the presence of SARS-CoV-2 RNA using the AmpliTest SARS-CoV-2 reagent kit (Federal State Budgetary Institution “Center for Strategic Planning and Management of Medical and Biological Health Risks” of the Federal Medical and Biological Health Organization of Russia) according to the manufacturer’s instructions.

**Table 1.** Mean threshold cycles ( $C_t$ ) for the *ACE2* gene in samples obtained from the lungs of mice after the introduction of AAV vectors

Vector	Dose <sup>a</sup>	Mean value of the threshold cycle, $C_t$		
		time, days		
		7	14	21
AAV9	$6 \times 10^{10}$	$19.7 \pm 0.8$	$19.2 \pm 1.0$	$20.3 \pm 0.1$
	$2 \times 10^{10}$	$23.3 \pm 1.8$	$20.4 \pm 0.3$	$20.2 \pm 0.3$
	$6 \times 10^9$	$21.0 \pm 0.5$	$21.7 \pm 0.4$	$20.1 \pm 0.8$
AAV6	$2 \times 10^{10}$	$30.4 \pm 1.6$	$30.2$ (1 out of 3) <sup>b</sup>	$30.5 \pm 0.2$ (2 out of 3) <sup>b</sup>
	$6 \times 10^9$	$31.6$ (1 out of 3) <sup>b</sup>	$33.2$ (1 out of 3) <sup>b</sup>	$34.3$ (1 out of 3) <sup>b</sup>
AAV-DJ	$2 \times 10^{10}$	$21.7 \pm 2.0$	$20.3 \pm 1.4$	$21.1 \pm 1.1$
	$6 \times 10^9$	$21.0 \pm 0.5$	$23.0 \pm 1.6$	$20.5 \pm 0.5$

<sup>a</sup> The dose is given in terms of AAV genomic equivalents administered to one animal. <sup>b</sup> The number of PCR-positive samples for which the mean value of  $C_t$  was calculated.

**Morphological study.** The right lung of mice was fixed in 10% neutral buffered formalin for 24 h, dehydrated, and embedded in Histomix (BioVitrum, Russia). At the pouring stage, the material was oriented along the long axis. Serial sections 3 – 5  $\mu$ m thick were made on a Leica RM 2125 RTS rotary microtome (Leica, Germany), then stained with hematoxylin and eosin, and embedded in Canada balsam. Histological preparations were examined under a BX 51 light microscope (Olympus, Japan) with a material photo registration system.

**Statistical processing.** For quantitative data, the group arithmetic mean and standard error of the mean were calculated. Statistical analysis was performed using the Statistica 8.0 software. The significance of differences between data groups was assessed using Mann–Whitney *U* test. Differences were considered significant for  $p < 0.05$ .

## RESULTS

### *Expression of the ACE2 Gene in the Lungs of Mice After the Introduction of the Vector*

To obtain model mice with transient expression of hACE2, it is necessary to deliver the *ACE2* gene into lung cells. Following intranasal administration, the AAV vector, upon inhalation, enters the lower respiratory tract and transduces lung epithelial cells. *ACE2* expression in these cells leads to the appearance of hACE2 on their surface, and hence to the possibility of binding the SARS-CoV-2 virus to them. After binding to hACE2, the virus enters the cell and starts the replication cycle.

For intranasal administration, we used a modified version of a technique by L. Santry et al. [9]. The first experiment compared the expression of hACE2 in the

lungs of animals when used to deliver *ACE2* AAV with capsids of three different serotypes: AAV9, AAV6 and AAV-DJ. AAV-vectors in the doses indicated in Table 1 were administered to mice according to the procedure described above. The AAV vector of each serotype was administered to a group of nine animals. On days 7, 14 and 21 after AAV administration, lungs from three mice were harvested and the amount of hACE2 mRNA was assessed using reverse transcription (RT) with real-time PCR. Also, to assess the efficiency of RNA extraction and RT-PCR, the mRNA level of mouse beta-glucuronidase (*Gusb*) was measured in the samples. Average threshold cycle ( $C_t$ ) for *Gusb* mRNA was 18.4, and the standard deviation for  $C_t$  in samples from different animals did not exceed 7%, which made it possible to compare the results of measuring hACE2 mRNA without normalization, using  $C_t$  values as a comparison parameter for *ACE2*.

As can be seen from the data given in Table 1, introduction *ACE2* using the AAV6 vector led to the expression of this gene at a very low level in some animals, while hACE2 mRNA could not be detected at all in the rest. After the introduction of the *ACE2* gene using the AAV9 and AAV-DJ vectors, its stable expression in the lungs was observed. *ACE2* expression level did not differ significantly when delivered by the AAV9 and AAV-DJ vectors. When comparing the amount of hACE2 mRNA in the lungs of mice with the introduction of different doses of vectors (from  $6 \times 10^9$  up to  $6 \times 10^{10}$  for AAV9 vector and from  $6 \times 10^9$  up to  $2 \times 10^{10}$  for the AAV-DJ vector) it was found that the *ACE2* expression differed slightly and remained at the same level for up to 21 days. For further experiments, the AAV-DJ vector was chosen, since it gave a higher yield during production.

**Table 2.** Design of the experiment to infect mice with SARS-CoV-2

No. <sup>a</sup>	Number of mice	Time, days					
		1	10	14 (4 dpi <sup>d</sup> )		17 (7dpi <sup>d</sup> )	
		vector introduction <sup>b</sup>	infection <sup>c</sup>	left lung	right lung	left lung	right lung
1	3	—	—	n.t. <sup>e</sup>	n.t.	n.t.	Histology
2	6	+	—	RNA <sup>f</sup>	IT <sup>g</sup>	RNA IT	Histology
3	6	+	+	RNA	IT	RNA IT	Histology
4	6	—	+	RNA	IT	RNA IT	Histology

<sup>a</sup> Group number; <sup>b</sup> vector AAV-DJ-hACE2 at a dose of  $2 \times 10^{10}$  administered to mice intranasally; <sup>c</sup> mice were infected with the SARS-CoV-2 virus; <sup>d</sup> (day post-infection)—day after infection; in each group, lungs were taken from three animals; <sup>e</sup> lungs were not taken; <sup>f</sup> determination of SARS-CoV-2 RNA; <sup>g</sup> infectious titer of SARS-CoV-2.

#### *Development of SARS-CoV-2 Infection in Transduced AAV-DJ-hACE2 mice*

The design of the experiment to study the development of infection caused by SARS-CoV-2 in transduced and non-transduced animals is presented in Table 2.

On the 4th and 7th days after infection, the lungs were taken from the animals to determine the infectious titer of the virus, SARS-CoV-2 RNA and for histological examination—in accordance with Table 2.

The results of measuring the infectious titer of SARS-CoV-2 in the lungs are shown in Table 3. In uninfected group 2, all samples were negative. In group 3, transduced with AAV-DJ-hACE2, on the fourth day after infection, the infectious titer Ig TCID<sub>50</sub>/mL averaged  $3.08 \pm 0.14$  log. At the same time, in animals of group 4—not transduced with the vector—the titer was an order of magnitude lower and amounted to  $2.08 \pm 0.14$  log. In animals receiving AAV-DJ-hACE2, the infectious titer decreased from  $3.08 \pm 0.14$  log on the fourth day up to  $2.17 \pm 0.14$  log on the seventh day, and in group 4 on the seventh day the virus was not detected at all.

When testing SARS-CoV-2 RNA using the SARS-CoV-2 AmpliTest kit by real-time RT-PCR, RNA isolation and analysis quality were assessed by internal control, the spread of C<sub>t</sub> did not exceed 1, which made it possible to compare the values of C<sub>t</sub> for SARS-CoV-2 RNA without normalization. On the fourth day, there were no significant differences in the level of SARS-CoV-2 RNA between groups 3 and 4. Samples from all three mice in group 3 were positive—mean C<sub>t</sub> was 26.7. In group 4, one of the three samples was negative, for the remaining groups the C<sub>t</sub> values were 24.8 and 26.8. SARS-CoV-2 RNA was not detected in the samples obtained on the seventh day, with the exception of one

sample from group 3, where a low level was detected (C<sub>t</sub> = 29.1)

#### *Morphological Study of the Lungs of Mice*

On the 17th day of the experiment (7th day after infection with SARS-CoV-2 of groups 3 and 4), a morphological study of the lungs was performed in some animals. It was shown that the lungs of intact mice (group 1) and mice of group 2 (17 days after administration of AAV-DJ-hACE2) had a normal structure (Figs. 1a–1d). On the 7th day after infection with SARS-CoV-2 in mice from group 4 (not transduced with AAV-DJ-hACE2), the histostructure of the lungs was generally normal. However, in the wall of individual bronchi and in the connective tissue around individual vessels, small lymphohistiocytic accumulations were detected (Figs. 1e, 1f).

In the microscopic examination of the lungs of mice from group 3 (which received AAV-DJ-hACE2)—on the 7th day after infection with SARS-CoV-2—in two out of three mice, areas with pronounced alterative and inflammatory changes were found. In the lung of one mouse, airless foci and areas with reduced airiness occupied 60–70% of the cut area, and in another, 25–30% (Fig. 2a). Bronchial lumens in these foci were filled with purulent exudate. The epithelial lining of the bronchi contained cells with dystrophic changes, some of the epitheliocytes were desquamated into the lumen due to the cytopathic effect of the coronavirus. The lamina propria of the bronchial mucosa was moderately infiltrated with lymphocytes, histiocytes and neutrophils (Fig. 2b). In the adventitial layer of the bronchi, hyperplasia of broncho-associated lymphoid tissue (BALT) was noted. In the peribronchial alveolar ducts, alveoli and perivascularly, a pronounced inflammatory infiltration from lymphocytes and histiocytes was detected, alternating with exten-

**Table 3.** Analysis of infectious titer and SARS-CoV-2 RNA in mouse lungs

Group	mouse no.	Time, days			
		4dpi		7dpi	
		virus titer, log(TCID <sub>50</sub> )	Viral RNA, C <sub>t</sub>	virus titer, log(TCID <sub>50</sub> )	Viral RNA, C <sub>t</sub>
1	1			n.d. <sup>a</sup>	n.d.
	2			n.d.	n.d.
	3			n.d.	n.d.
2 (+AAV-DJ-hACE2)	1	— <sup>b</sup>	—	—	—
	2	—	—	—	—
	3	—	—	—	—
3 (+AAV-DJ-hACE2 +SARS-CoV-2)	1	3.25	28.4	2.25	29.1
	2	3.0	24.1	2.25	—
	3	3.0	27.5	2.0	—
	Mean	<b>3.08 ± 0.14</b>	<b>26.7 ± 2.3</b>	<b>2.17 ± 0.14</b>	
4 (+SARS-CoV-2)	1	2.0	—	n.d.	—
	2	2.25	24.8	n.d.	—
	3	2.0	26.8	n.d.	—
	Mean	<b>2.08 ± 0.14</b>			

<sup>a</sup> Not determined; <sup>b</sup> negative result.

sive areas of purulent inflammation, in which the lumen of the alveoli and interalveolar septa were not determined (Fig. 2c). In areas outside of pneumonia, hyperemia of blood vessels, pronounced hyperplasia of BALT and perivascular lymphoid tissue were visible (Fig. 2d). Thus, on the seventh day after intranasal infection of SARS-CoV-2 mice expressing hACE2, airless areas of the parenchyma were detected in the lungs of animals, corresponding to bacterial-viral bronchopneumonia, with the onset of abscess formation.

## DISCUSSION

None of the animal models used today to simulate COVID-19 can be considered ideal and fully reflect the course of infection in humans. A widely used model of the disease in Syrian hamsters supports the replication of the virus and causes a pathological process in the lungs of animals, but does not lead to death. Using mice has its advantages. Mice are the most common small laboratory animals and are cheaper and more convenient for large-scale research. An important advantage of mice is the ability to study in detail the T-cell response, both in terms of its development during COVID-19 infection and after vaccination [11]. Of great interest is the “lethal model” of transgenic mice, in the genome of which the gene encoding human ACE2—*ACE2* is inserted but access to such animals is limited.

Attempts to provide *ACE2* transient expression have been made to create a mouse model capable of infection by both SARS-CoV-1 and SARS-CoV-2. For *ACE2* gene delivery an adenoviral vector or adeno-associated vectors were used [2–4, 12]. C.-P. Sun et al. [12] showed that intranasal administration of AAV6-hACE2 to mice leads to low transduction rate, while intratracheal administration leads to high efficiency of transduction of lung cells. L. Santry et al. [9] proposed a modified method of intranasal administration, which allowed efficient delivery of the AAV6 vector with the GFP marker gene to the lungs of mice. We also used a modified technique for intranasal administration of AAV. However, administration of the AAV6-hACE2 vector resulted in very low or undetectable levels of hACE2 expression in the lungs of mice. At the same time, the use of vectors of other serotypes: AAV9 and AAV-DJ—allowed successful transduction of lung cells and a high and reproducible level of *ACE2* expression. Thus, we managed to avoid the problems associated with the use of intratracheal vector injection, a complex and invasive method that leads to large variability in results.

When animals transduced with AAV-DJ-hACE2 were infected with SARS-CoV-2, the virus effectively replicated in the lungs of model mice: the infectious titer on day 4 was 3.08 log and on day 7 decreased to 2.17 log. These data are somewhat different from the results obtained by B. Israelow et al. [3], who showed complete elimination of the infectious virus from the

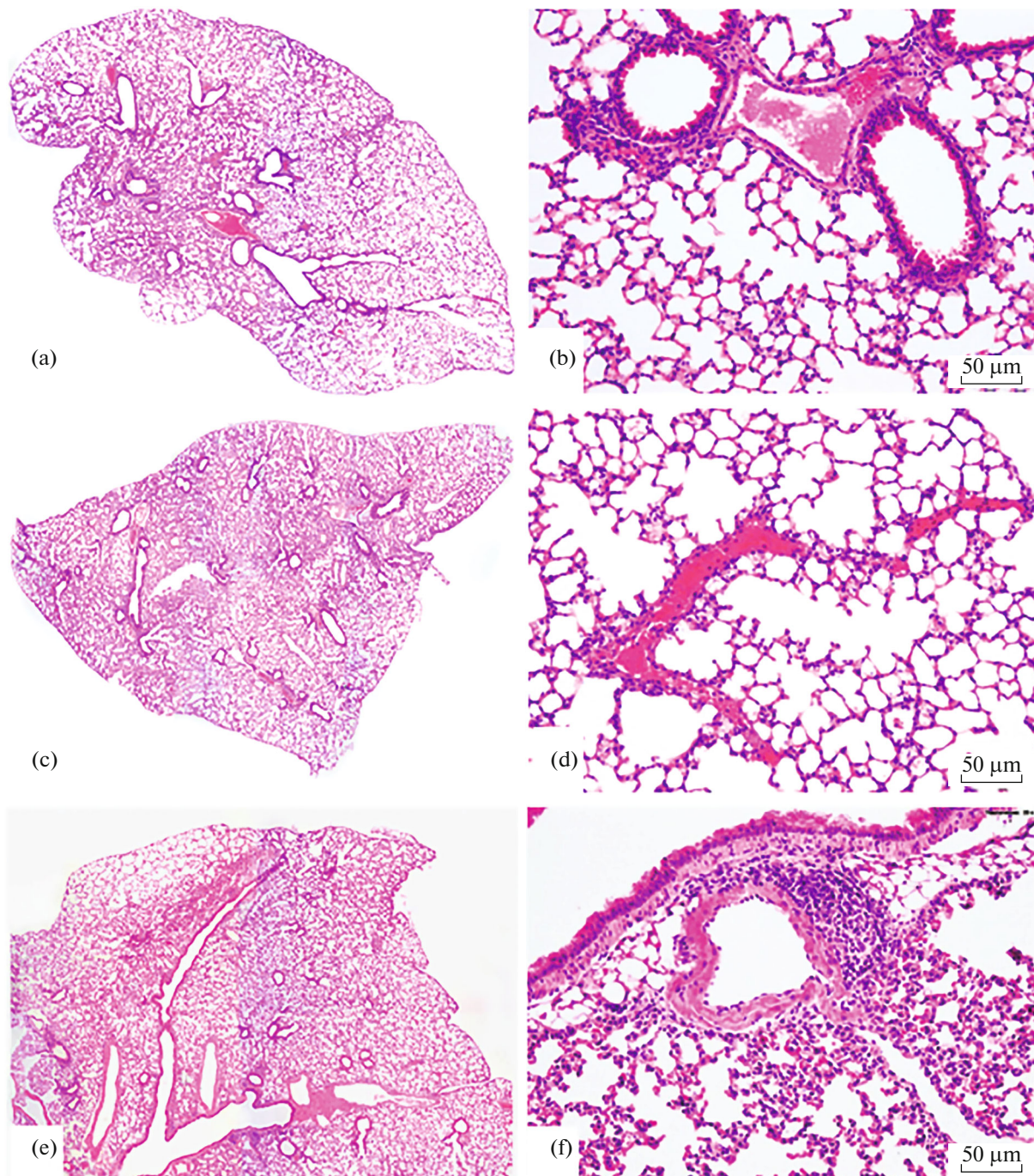


**Fig. 1.** Morphological characteristics of the lungs of mice on the 17th day of the experiment. The lungs of animals from the control group 1 (a, b), from group 2 (17 days after administration of AAV-DJ-hACE2) (c, d) and from group 4 (day 7 post infection with SARS-CoV-2) (e, f) are shown. In the lungs of animals of groups 1 and 2 (a–d) the lumen of the bronchi is free, single lymphocytes are visible in the wall, air gaps of the alveolar ducts and alveoli, and thin interalveolar septa. In group 4, small lymphohistiocytic accumulations are located in the wall of the bronchus and perivascularly. Stained with hematoxylin and eosin; magnification:  $\times 40$  (a, c, e) and  $\times 200$  (b, d, f).

lungs on day 7 using a similar model. An unexpected result was the detection of infectious virus in a low titer in animals that were not injected with AAV-hACE2, on the 4th day after infection with SARS-CoV-2.

The data on the detection of viral RNA turned out to be less informative than the results on the determination of the infectious titer: on the 4th day after infection, viral RNA was detected both in the group of mice

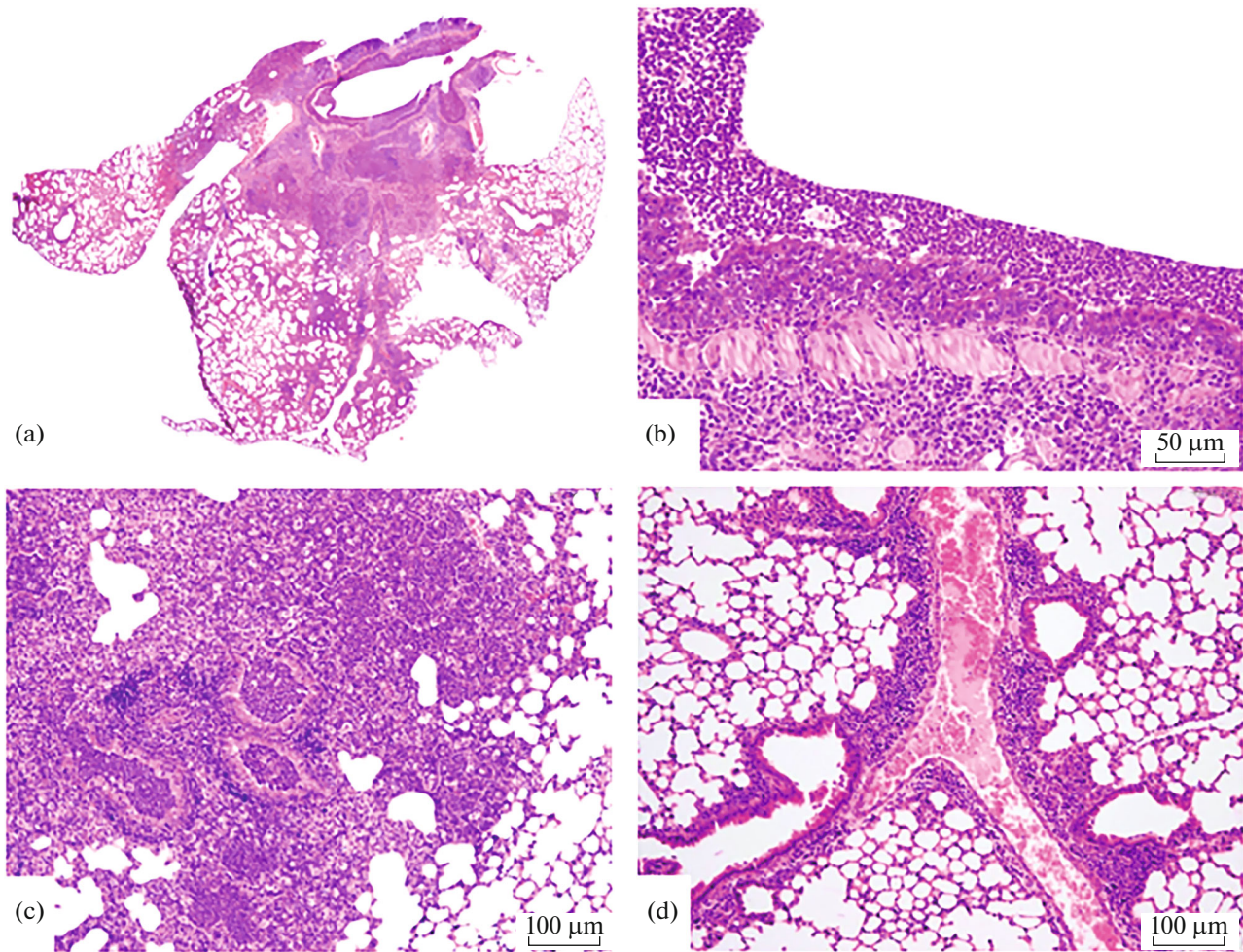


**Fig. 2.** Morphological characteristics of the lungs of mice from group 3 transduced with AAV-DJ-hACE2 and infected with SARS-CoV-2 on the 17th day of the experiment. (a) Picture of bronchopneumonia; (b) the lumen of the large bronchus contains purulent exudate, epithelium with dystrophic changes, leukopedesis, inflammatory infiltration of the wall; (c) the focus of bronchopneumonia: the lumen of the bronchi, bronchioles and alveoli are filled with purulent exudate with a significant admixture of macrophages; (d) zone outside bronchopneumonia: muff-like perivascular lymphohistiocytic infiltrate, hyperplasia of BALT, plethora of the vessel. Stained with hematoxylin and eosin. Increase:  $\times 40$  (a),  $\times 200$  (b),  $\times 100$  (c, d).

that received AAV-DJ-hACE2 and in the group without AAV-DJ-hACE2. The fact that viral RNA can circulate in mice that do not support SARS-CoV-2 replication was also demonstrated in previously published works [3, 13].

Replication of SARS-CoV-2 in the lungs of animals transduced with AAV-DJ-hACE2 led to the development of bacterial-viral bronchopneumonia on the 7th day after infection, in contrast to animals that did not receive AAV-DJ-hACE2. The addition of bacterial microflora was probably facilitated by an impairment of the integrity of the mucociliary barrier of the airways, due to the direct effect of the virus on the ciliated epithelium of the bronchi. No pathological changes were found in the lungs of non-transduced mice on the 7th day after infection with SARS-CoV-2.

Thus, our experiments demonstrated the possibility of quickly obtaining a relevant model of mice that are susceptible to infection with SARS-CoV-2 and can be used to study the effectiveness of vaccines and drugs under development for the prevention and treatment of COVID-19.

The model presented can be further improved to obtain a “lethal model” of SARS-CoV-2 infection, which is most in demand for the study of vaccines and drugs. An interesting avenue for model optimization could be the administration of AAV-hACE2 to humanized mice. The use of such mice makes it possible to more accurately mimic the clinical manifestations of COVID-19 in humans, in particular, the chronic disease course, the development of pulmonary fibrosis, and systemic lymphopenia [13].

## ACKNOWLEDGMENTS

The work was performed using the equipment of the Center for Collective Use of the I.I. Mechnikov Research Institute of Vaccines and Serums.

## FUNDING

The study was carried out with the financial support of the Russian Foundation for Basic Research within the framework of scientific project No. 20-04-60100. The work was performed using the equipment of the Center for Collective Use of the I.I. Mechnikov Research Institute of Vaccines and Serums.

## COMPLIANCE WITH ETHICAL STANDARDS

*Conflict of interests.* The authors declare that they have no conflicts of interest.

*Statement on the welfare of animals.* All work with animals was carried out in accordance with the rules adopted by the European Convention for the Protection of Vertebrate Animals (Strasbourg, 1986); Order of the Ministry of Health of the Russian Federation No. 199N dated April 1, 2016, Principles of Good Laboratory Practice (OECD, ENV/MC/CUEM (98)17, 1997); GOST 33044-2014 “Principles of Good Laboratory Practice” (identical to GLP OECD); Good Laboratory Practice for Nonclinical Laboratory Studies (21 CFR Part 58, 1978, USA, FDA), reviewed and approved by the commission of the Federal State Budget Scientific Institution “I.I. Mechnikov Research Institute for Vaccines and Serums” for the care and use of animals for compliance with regulatory acts.

## REFERENCES

- Winkler E.S., Bailey A.L., Kafai N.M., Nair S., McCune B.T., Yu J., Fox J.M., Chen R.E., Earnest J.T., Keeler S.P., Ritter J.H., Kang L.I., Dort S., Robichaud A., Head R., Holtzman M.J., Diamond M.S. 2020. SARS-CoV-2 infection of human ACE2-transgenic mice causes severe lung inflammation and impaired function. *Nat. Immunol.* **21** (11), 1327–1335.
- Hassan A.O., Case J.B., Winkler E.S., Thackray L.B., Kafai N.M., Bailey A.L., McCune B.T., Fox J.M., Chen R.E., Alsoussi W.B., Turner J.S., Schmitz A.J., Lei T., Shrihari S., Keeler S.P., Fremont D.H., Greco S., McCray P.B., Jr., Perlman S., Holtzman M.J., Eilebedy A.H., Diamond M.S. 2020. A SARS-CoV-2 infection model in mice demonstrates protection by neutralizing antibodies. *Cell.* **182** (3), 744–753. e4.
- Israelow B., Song E., Mao T., Lu P., Meir A., Liu F., Alfajaro M.M., Wei J., Dong H., Homer R.J., Ring A., Wilen C.B., Iwasaki A. 2020. Mouse model of SARS-CoV-2 reveals inflammatory role of type I interferon signaling. *J. Exp. Med.* **7**, 217 (12), e20201241.
- Sun J., Zhuang Z., Zheng J., Li K., Wong R. L., Liu D., Huang J., He J., Zhu A., Zhao J., Li X., Xi Y., Chen R., Alshukairi A.N., Chen Z., Zhang Z., Chen C., Huang X., Li F., Lai X., Chen D., Wen L., Zhuo J., Zhang Y., Wang Y., Huang S., Dai J., Shi Y., Zheng K., Leidinger M.R., Chen J., Li Y., Zhong N., Meyerholz D.K., McCray P.B. Jr, Perlman S., Zhao, J. 2020. Generation of a broadly useful model for COVID-19 pathogenesis, vaccination, and treatment. *Cell.* **182** (3), 734–743.
- Chan K.K., Dorosky D., Sharma P., Abbasi S.A., Dye J.M., Kranz D.M., Herbert A.S., Procko E. 2020. Engineering human ACE2 to optimize binding to the spike protein of SARS coronavirus 2. *Science.* **369** (6508), 1261–1265.
- Higuchi R., Krummel B., Saiki R. 1988. A general method of *in vitro* preparation and specific mutagenesis of DNA fragments: study of protein and DNA interactions. *Nucleic Acids Res.* **16** (15), 7351–7367.
- Kimura T., Ferran B., Tsukahara Y., Shang Q., Desai S., Fedoce A., Pimentel D.R., Luptak I., Adachi T., Ido Y., Matsui R., Bachschmid M.M. 2019. Production of adeno-associated virus vectors for in vitro and in vivo applications. *Sci. Rep.* **9** (1), 13601.
- Aurnhammer C., Haase M., Muether N., Hausl M., Rauschhuber C., Huber I., Nitschko H., Busch U., Sing A., Ehrhardt A., Baiker A. 2012. Universal real-time PCR for the detection and quantification of adeno-associated virus serotype 2-derived inverted terminal repeat sequences. *Hum. Gene Ther. Methods.* **23** (1), 18–28.
- Santry L.A., Ingrao J.C., Yu D.L., de Jong J.G., van Lieshout L.P., Wood G.A., Wootton S.K. 2017. AAV vector distribution in the mouse respiratory tract following four different methods of administration. *BMC Biotechnol.* **17** (1), 43.
- Ramakrishnan M.A. 2016. Determination of 50% endpoint titer using a simple formula. *World J. Virol.* **5** (2), 85–86.
- Veit S., Jany S., Fux R., Sutter G., Volz A. 2018. CD8+ T cells responding to the middle east respiratory syndrome coronavirus nucleocapsid protein delivered by vaccinia virus MVA in mice. *Viruses.* **10** (12), 718.
- Sun C.-P., Jan J.-T., Wang I.-H., Ma H.-H., Ko H.-Y., Wu P.-Y., Kuo T.-J., Liao H.-N., Lan Y.-H., Sie Z.-L., Chen Y.-H., Ko Y.-A., Liao C.-C., Chen L.-Y., Lee I.-J., Tsung S.-I., Lai Y.-J., Chiang M.-T., Liang J.-J., Liu W.-C., Wang J.-R., Yuan J.P.-Y., Lin Y.-S., Tsai Y.-C., Hsieh S.-L., Li C.-W., Wu H.-C., Ko T.-M., Lin Y.-L., Tao M.-H. 2021. Rapid generation of mouse model for emerging infectious disease with the case of severe COVID-19. *PLoS Pathog.* **17** (8), e1009758.
- Sefik E., Israelow B., Mirza H., Zhao J., Qu R., Kaffe E., Song E., Halene S., Meffre E., Kluger Y., Nussenzweig M., Wilen C.B., Iwasaki A., Flavell R.A. 2022. A humanized mouse model of chronic COVID-19. *Nat. Biotechnol.* **40**, 906–920. <https://doi.org/10.1038/s41587-021-01155-4>